AD-A182 437 STUDIES OF BORON IMPLANTATION THROUGH PHOTOCHEMICALLY 1/1
DEPOSITED SIO2 FILM (U) AEROSPACE CORP EL SEGUNDO CA
CHEMISTRY AND PHYSICS LAB R C BOWMAN ET AL 22 MAY 87

UNCLASSIFIED TR-0086(6945-77)-3 SD-TR-87-26 F/G 20/12 NL

END
8-87
DTIC

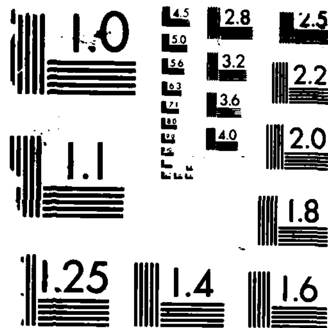
1.0
1.1
1.25
1.4
1.6
1.8
2.0
2.2
2.5
2.8
3.2
3.6
4.0
4.5
5.0
5.6
6.3
MICROCOPY RESOLUTION TEST CHART
NATIONAL BUREAU OF STANDARDS-1963-A

REPORT SD-TR-87-26

(12)

DTIC FILE COPY

AD-A182 437

Studies of Boron Implantation Through Photochemically Deposited SiO_2 Films on $Hg_{1-x}Cd_xTe$

R. C. BOWMAN, JR., R. E. ROBERTSON,
and J. F. KNUDSEN
Chemistry and Physics Laboratory
Laboratory Operations
The Aerospace Corporation
El Segundo, CA 90245

and

R. G. DOWNING
Center for Analytical Chemistry
National Bureau of Standards
Gaithersburg, MD 20899

DTIC
ELECTE
JUL 15 1987
S D
D

22 May 1987

Prepared for

SPACE DIVISION
AIR FORCE SYSTEMS COMMAND
Los Angeles Air Force Station
P.O. Box 92960, Worldway Postal Center
Los Angeles, CA 90009-2960

APPROVED FOR PUBLIC RELEASE.
DISTRIBUTION UNLIMITED

This report was submitted by The Aerospace Corporation, El Segundo, CA 90245, under Contract No. F04701-85-C-0086 with the Space Division, P.O. Box 92960, Worldway Postal Center, Los Angeles, CA 90009-2960. It was reviewed and approved for The Aerospace Corporation by S. Feuerstein, Director, Chemistry and Physics Laboratory. Lt Walter E. Leyland, SD/CNDA, was the project officer for the Mission-Oriented Investigation and Experimentation (MOIE) program.

This report has been reviewed by the Public Affairs Office (PAS) and is releasable to the National Technical Information Service (NTIS). At NTIS, it will be available to the general public, including foreign nationals.

This technical report has been reviewed and is approved for publication. Publication of this report does not constitute Air Force approval of the report's findings or conclusions. It is published only for the exchange and stimulation of ideas.

WALTER E. LEYLAND, Lt, USAF
MOIE Project Officer
SD/CNDA

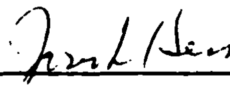

JOSEPH HESS, GM-15
Director, AFSTC West Coast Office
AFSTC/WCO OL-AB

REPORT DOCUMENTATION PAGE

Field	Content
1a. REPORT SECURITY CLASSIFICATION	Unclassified
1b. RESTRICTIVE MARKINGS	A182437
2a. SECURITY CLASSIFICATION AUTHORITY	
2b. DECLASSIFICATION/DOWNGRADING SCHEDULE	
3. DISTRIBUTION/AVAILABILITY OF REPORT	Approved for public release; distribution unlimited.
4. PERFORMING ORGANIZATION REPORT NUMBER(S)	TR-0086(6945-07)-3
5. MONITORING ORGANIZATION REPORT NUMBER(S)	SD-TR-87-26
6a. NAME OF PERFORMING ORGANIZATION	The Aerospace Corporation Laboratory Operations
6b. OFFICE SYMBOL (If applicable)	
7a. NAME OF MONITORING ORGANIZATION	
6c. ADDRESS (City, State and ZIP Code)	El Segundo, CA 90245
7b. ADDRESS (City, State and ZIP Code)	
8a. NAME OF FUNDING/SPONSORING ORGANIZATION	Space Division
8b. OFFICE SYMBOL (If applicable)	
9. PROCUREMENT INSTRUMENT IDENTIFICATION NUMBER	F04701-85-C-0086
8c. ADDRESS (City, State and ZIP Code)	Los Angeles Air Force Station Los Angeles, CA 90009-2960
10. SOURCE OF FUNDING NOS.	PROGRAM ELEMENT NO. / PROJECT NO. / TASK NO. / WORK UNIT NO.
11. TITLE (Include Security Classification)	Studies of Boron Implantation through
12. PERSONAL AUTHOR(S)	Bowman, Robert C., Jr., Robertson, Ruby E., Knudsen, John F., and Downing, R. G. (NBS)
13a. TYPE OF REPORT	
13b. TIME COVERED	FROM ____ TO ____
14. DATE OF REPORT (Yr., Mo., Day)	1987 May 22
15. PAGE COUNT	17
16. SUPPLEMENTARY NOTATION	Certain commercial equipment, instruments, or materials are identified in this report in order to adequately specify the experimental procedure. Such identification does not imply recommendation or endorsement by the National Bureau of Standards,
17. COSATI CODES	FIELD / GROUP / SUB. GR.
18. SUBJECT TERMS (Continue on reverse if necessary and identify by block number)	Mercury cadmium tellurides, Ion implantation effects, Silicon dioxide passivation, Neutron depth profiling, infrared materials, analysis

19. ABSTRACT (Continue on reverse if necessary and identify by block number)

Variable temperature Hall and resistivity measurements have been used to monitor the changes in carrier behavior in p-type $Hg_{1-x}Cd_xTe$ when boron ions are implanted through photochemically deposited SiO_2. The formation of an n-type layer is demonstrated. Quantitative and non-destructive determinations of the absolute ^{10}B concentration and distribution have been obtained by the novel method of neutron depth profiling. As expected, the boron distributions in the SiO_2 films and $Hg_{1-x}Cd_xTe$ are strongly dependent upon the ion implant energy. However, negligible changes in the boron depth profiles were found after 200°C anneals. The present results are briefly related to the performance behavior of mid-wavelength infrared (MWIR) sensors produced via generic ion implantation procedures.

Field	Content
20. DISTRIBUTION/AVAILABILITY OF ABSTRACT	UNCLASSIFIED/UNLIMITED ☒ SAME AS RPT ☐ DTIC USERS ☐
21. ABSTRACT SECURITY CLASSIFICATION	Unclassified
22a. NAME OF RESPONSIBLE INDIVIDUAL	
22b. TELEPHONE NUMBER (Include Area Code)	
22c. OFFICE SYMBOL	

11. (Continued) Photochemically Deposited SiO_2 Films on $Hg_{1-x}Cd_xTe$

16. (Continued) nor does it imply that the materials or equipment identified are necessarily the best available for the purpose.

18. (Continued) Boron implant profiles

PREFACE

We wish to thank Dr. R. Alt, Dr. J. Marks, and R. Egler for performing the ellipsometry measurements and E. Fletcher for assistance with the Hall measurements.

Accesion For
NTIS CRA&I
DTIC TAB
Unannounced
Justification
By
Distribution /
Availability Codes
Dist | Avail and / or Special
A-1

CONTENTS

PREFACE 1

I. INTRODUCTION 7

II. SAMPLE DESCRIPTION 9

III. RESULTS AND DISCUSSIONS 11

A. HALL MEASUREMENTS 11

B. NEUTRON DEPTH PROFILES 14

VI. CONCLUSIONS 21

REFERENCES 23

FIGURES

1. Temperature dependences of resistivity and Hall coefficients for p-$Hg_{0.7}Cd_{0.3}Te$ epilayer before and after the $^{11}B^{+}$ implants 12

2. Comparisons of ratios for electron concentration (N_e) and mobility (μ_e) after boron implants through nominal 100 nm SiO_2 films and bare surface 13

3. ^{10}B profiles for $Hg_{0.68}Cd_{0.32}Te$ sample NDP-3 as implanted and after 1 hr 200°C anneal 17

4. ^{10}B profiles for PC-SiO_2 coated $Hg_{0.68}Cd_{0.32}Te$ sample NDP-2 as implanted, after 1 hr 200°C anneal, and after buffered HF etch to remove SiO_2 film 17

5. Comparison of ^{10}B profiles for different implant energies 18

6. Measured ^{10}B profiles for as-implanted 250 keV $^{10}B^{+}$ ions in bulk sample NDP-5 and epitaxial sample NDP-7 18

TABLES

1. Summary of $Hg_{1-x}Cd_xTe$ Samples used in Neutron Depth Profiling Experiments 9

2. Comparisons of NDP Measured ^{10}B Contents in Implanted $Hg_{0.7}Cd_{0.3}Te$ Samples 15

I. INTRODUCTION

Ion implantation has been widely utilized[1-3] for the formation of diode junctions during the fabrication of $Hg_{1-x}Cd_xTe$ infrared sensor photovoltaic devices. Due to the light masses of the boron isotopes which produce deep junctions at modest acceleration energies as well as their expected donor character when on metal sites, the implanted species are often boron ions. The production of photodiodes via ion implantation involves numerous processing steps such as selective etching, contact deposition, and annealing. Because of the low stability of the $Hg_{1-x}Cd_xTe$ surfaces as well as inherent fragility of these crystals, passivation treatments with deposited thin films are usually included during the photodiode processing. Different research groups[4-6] have recently found that photochemically (PC) deposited SiO_2 films can give greatly improved electrical properties for the photodiodes when compared to materials covered by only native or anodic oxides. Since the specific microscopic causes for this improvement are not understood, the reproducibility of high quality SiO_2-passivated photodiodes has been less than initially expected.

In order to provide improved insights on the material property changes that occur when boron ions are implanted through PC-SiO_2 films on various $Hg_{0.7}Cd_{0.3}Te$ surfaces, several experimental studies have been initiated. The three techniques of present interest are neutron depth profiling (NDP) measurements[7,8] of the implanted boron (^{10}B) isotopes, variable temperature Hall effect and resistivity measurements to monitor the charge carrier parameters, and ellipsometry to determine the thicknesses of the PC-SiO_2 films. Some special advantages[9] of the NDP technique to measure the ^{10}B distributions are its nondestructive nature, relatively few interferences, good spatial resolution, and the ability to quantitatively examine interfacial regions such as between SiO_2 and $Hg_{1-x}Cd_xTe$. In contrast, the more commonly used secondary ion mass spectrometry (SIMS) technique often has great difficulty with analyses between two very dissimilar layers. Because NDP has been used much less frequently[7] on $Hg_{1-x}Cd_xTe$ than on other materials[9], various aspects of

this method will be discussed later in the report. The initial results indicate that NDP data on boron (^{10}B contents at the SiO_2-$Hg_{1-x}Cd_xTe$ interface can be correlated with Hall measurement of electron carriers produced by ion implantation.

II. SAMPLE DESCRIPTION

The nominal $Hg_{0.7}Cd_{0.3}Te$ samples include bulk single crystals from Cominco and approximately 15-20 μm thick liquid-phase epitaxially grown layers on <111>-oriented CdTe substrates. Some properties of the samples used in the NDP experiments are presented in Table 1. A model 400 MPR-Veeco/AI ion implanter was used to implant either $^{11}B^{+}$ or $^{10}B^{+}$ ions into electrically grounded samples at ambient temperature. The beam ion current was kept sufficiently low to avoid inadvertent heating effects during implantation. The implant energies are summarized in Table 1. The boron ions have been implanted through nominal 100 nm PC-SiO_2 films[4,5] as well as 5% bromine-methanol solution etched bare surfaces. The PC-SiO_2 film thicknesses for samples NDP-4, NDP-5, and NDP-7 have been measured by ellipsometry, whereas the SiO_2 thicknesses for samples NDP-1 and NDP-2 were obtained from the differences in the NDP curves following buffered HF-etches to remove the implanted SiO_2 films.

Table 1. Summary of $Hg_{1-x}Cd_xTe$ Samples Used in Neutron Depth Profiling Experiments

Sample I.D. Number	x	Form	Source	Implant Surface	SiO_2 Thickness (μm)	^{10}B Implant Energy (keV)	$^{10}B^{+}$ Dose (10^{15} ions/cm^2)
NDP-1	0.41(1)	Bulk	Cominco	SiO_2	0.105[a]	40/100	1.0/1.0
NDP-2	0.32(1)	Epi	Fermionics	SiO_2	0.105[a]	40/100	1.0/1.0
NDP-3	0.32(1)	Epi	Fermionics	Bare	0.00	40/100	1.0/1.0
NDP-4	0.41(1)	Bulk	Cominco	SiO_2	0.100	250	2.0
NDP-5	0.305(5)	Bulk	Cominco	SiO_2	0.109	250	2.0
NDP-6	0.33(2)	Epi	Rockwell	Bare	0.00	250	2.0
NDP-7	0.33(2)	Epi	Rockwell	SiO_2	0.107	250	2.0

[a]Estimated from NDP data as described in text.

III. RESULTS AND DISCUSSIONS

A. HALL MEASUREMENTS

The resistivities and Hall coefficients of epitaxial $Hg_{1-x}Cd_xTe$ samples before and after boron ion implantations were measured by the standard dc-method using a four-point van der Pauw configuration on nominal 3 mm squares. Ohmic electrical contacts were made by soldering In beads at the corners. The averaging scheme of Lou and Frye[10] was used to reduce any biases. The magnet current was reversed to generate the positive and negative magnetic fields of nominally 3.5 kG during the Hall measurements. A liquid helium transfer system was used with a digitally controlled heater on a copper block sample mount in a shielded all-metal cryostat to vary the sample temperature from a minimum of about 10 K to 300 K.

The resistivities and Hall coefficients for an initially p-type $Hg_{0.7}Cd_{0.3}Te$ Rockwell epilayer have been obtained before and after $^{11}B^{+}$ ion implantation (1×10^{14} ions/cm^2 at 40 keV and 1×10^{14} ions/cm^2 at 100 keV) and are compared in Figure 1. The temperature behavior of these parameters for both conditions is in very good agreement with previously published values[2,3,11,12] on similar materials. Figure 1 clearly illustrates that implantation creates a highly conductive n-type layer with very weak temperature dependence for electron density. Furthermore, the hole mobility (μ_h) at 80 K for the initial p-type layer is 290(10) cm^2/sV, which also agrees with literature values,[11,12] while an 80 K electron mobility (μ_e) of 9800(100) cm^2/sV was obtained from the implanted sample. The specific contributions of the implanted boron ions to the type conversion of $Hg_{1-x}Cd_xTe$ remains controversial,[1-3] and it is widely believed that unidentified defects created by the implantation are primarily responsible for the donor species in the n-layer.

The effects of implanting relatively low energy (i.e., 40 keV and 100 keV) boron ions through the PC-SiO_2 layer are illustrated in Figure 2. The ratios of the electron carrier concentrations (N_e) and mobilities are compared for as-implanted epilayers with and without the nominal 100 nm SiO_2-passivation film. While only a minor change in μ_e is observed over the

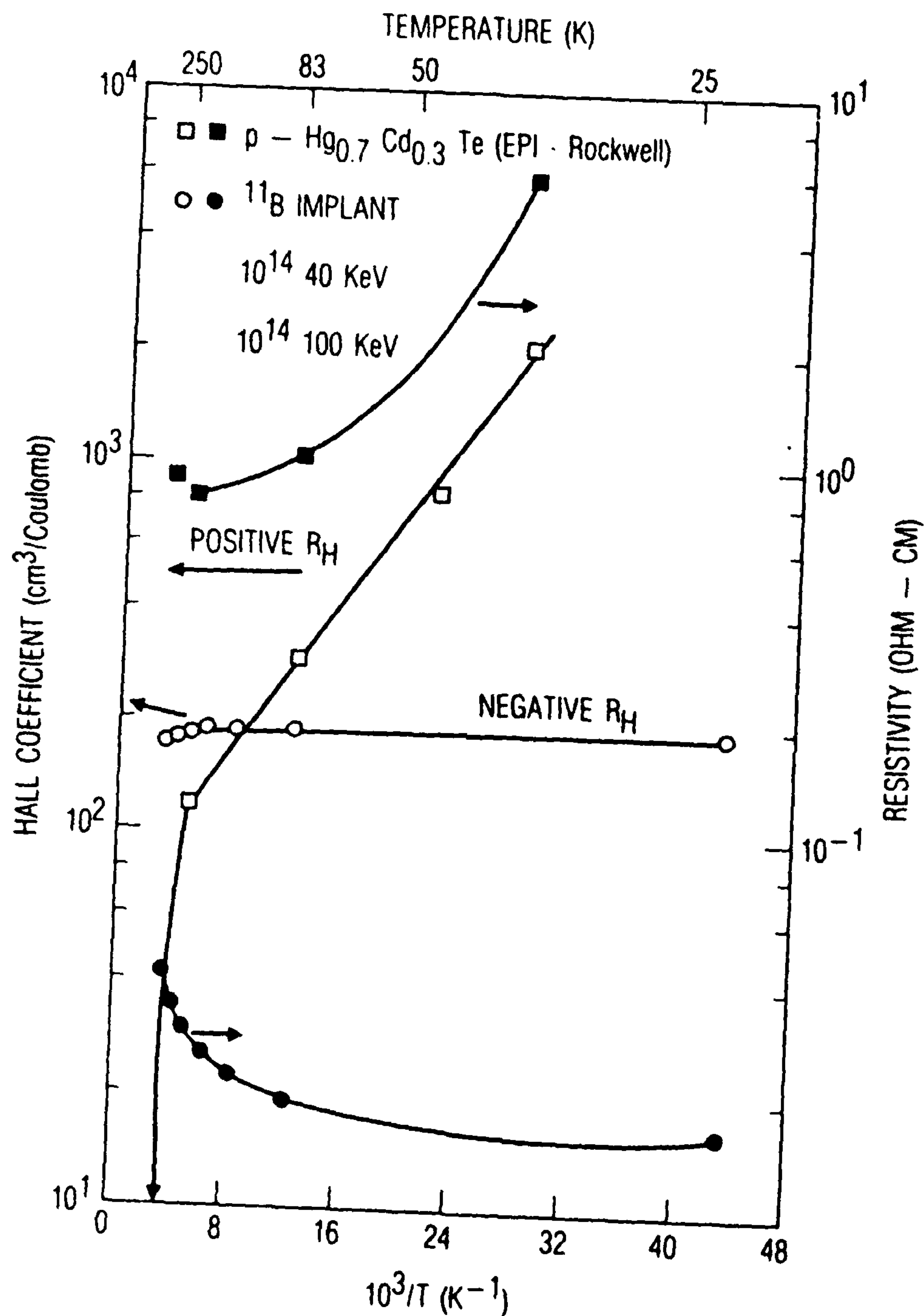

Fig. 1. Temperature dependences of resistivity and Hall coefficients for p-$Hg_{0.7}Cd_{0.3}Te$ epilayer before (squares) and after (circles) the $^{11}B^{+}$ implants.

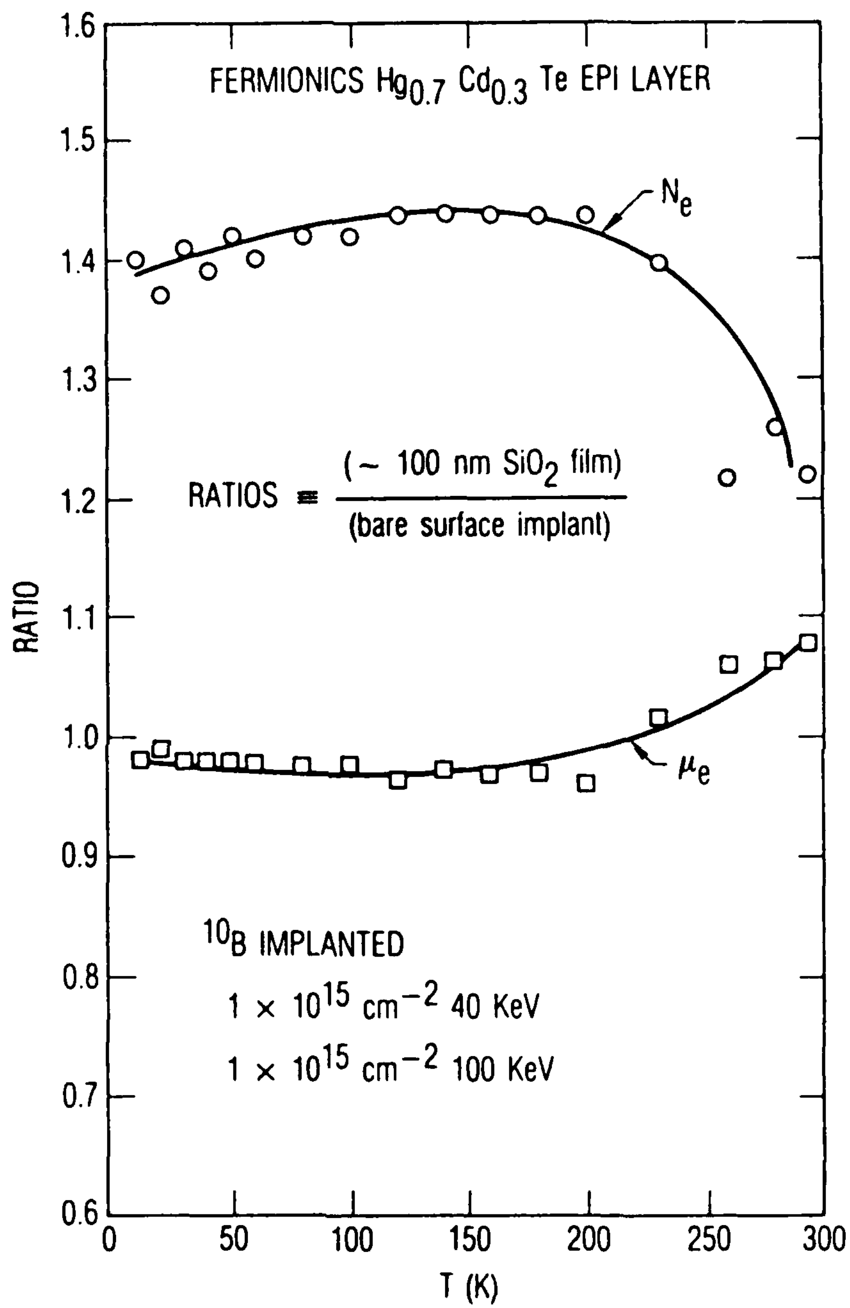

Fig. 2. Comparisons of ratios for electron concentration (N_e) and mobility (μ_e) after boron implants through nominal 100 nm SiO_2 films and bare surface.

entire temperature range, the Hall data below 250 K indicate that the surface carrier concentration is more than 40% larger for the PC-SiO_2 coated sample. The intrinsic donor contributions apparently reduce this difference as the temperatures approach 300 K. A tentative explanation for the enhanced N_e value in the PC-SiO_2 coated sample will be made when the NDP results on the boron profiles are presented.

B. NEUTRON DEPTH PROFILES

In NDP, the number and residual energy of charged particles emitted during neutron absorption reactions are measured to determine the concentration versus depth profile of individual nuclides.[13,14] The well-defined initial energy of charged particles (e.g., alphas or protons) and the recoil masses are given by the energy-mass conservation law $E = \Delta mc^2$. The difference between initial and detected residual energy is indicative of the reaction depth, whereas the number of charged particles detected at a given energy is proportional to the concentration of the parent nuclide at a given depth. With neutrons of thermal energies, only eight nuclides have absorption probabilities for charged particle emission greater than one barn where three are radioactive (i.e., ^{7}Be, ^{22}Na, and ^{59}Ni) and ^{40}K is of low natural abundance. The remaining favorable nuclides are ^{3}He, ^{6}Li, ^{10}B, and ^{14}N. Consequently, there is little opportunity for interference from an NDP analysis based on the $^{10}B(n, \alpha)\,^{7}Li$ reaction. Because NDP is a nuclear technique which is not subject to normal chemical or electrical effects, profiling across interfacial boundaries poses little difficulty. Furthermore, the method is nondestructive and capable of measuring absolute concentrations, which make it particularly attractive for comparison with other analytical methods.

The ^{10}B profiles in the $Hg_{1-x}Cd_xTe$ samples were obtained on the NDP facility[8] at the National Bureau of Standards 20 MW research reactor which uses a filtered beam of low-energy neutrons collimated into an approximately 1-cm-diameter circle to uniformly illuminate the investigated samples. The intensity of neutrons is about 6×10^8 cm^{-2} s^{-1} and gives a practical lower detection limit for ^{10}B in $Hg_{1-x}Cd_xTe$ of about 5×10^{13} atoms/cm^2 when

distributed within 5 μm below the surface. Profiles of the ^{10}B atoms have been obtained by NDP for all seven samples listed in Table 1. A thin aluminum mask with a 9.5 mm aperture was placed over the surface of each sample during these measurements. This permitted direct comparisons between the different sized specimens and a ^{10}B concentration standard. Because sample NDP-3 was estimated to be 10% smaller than the aperture in the mask, its concentration values, given in Table 2, are only used for relative comparison before and after a 200°C anneal.

Table 2. Comparisons of NDP Measured ^{10}B Contents in Implanted $Hg_{0.7}Cd_{0.3}Te$ Samples (Nominal Total Dose of 2.0×10^{15} B^{+} ions/cm^2)

Sample	Surface Film	NDP Measured Boron Contents (10^{15} atoms/cm^2) As Implanted	After 200°C Anneal	After Anneal and HF-Etch	% Boron in SiO_2 Film
NDP-1	SiO_2	1.98(6)	1.97(6)	1.46(4)	26
NDP-2	SiO_2	1.92(6)	1.92(6)	1.25(4)	35
NDP-3[a]	Bare	1.78(5)	1.75(5)	--	--

[a]This sample is about 10% smaller than charged-particle mask, and results were not corrected to reflect absolute concentration.

The full width at half-maximum (FWHM) depth resolution for ^{10}B in a material such as $Hg_{1-x}Cd_xTe$ would be estimated at less than 35 nm in a standard measurement configuration. However, the gold surface barrier silicon detectors used in NDP analyses are also sensitive to energetic electrons and to a much lesser degree the low-energy gamma rays. Since cadmium has an isotopically averaged cross section of 2520 ± 50 barns for the emission of energetic electrons and gamma rays, this element produces a broad, intense, low-energy background that rises exponentially at the low-energy end of the spectra and generates "pulse pile-up" effects in the measured ^{10}B alpha emission spectra. The pulse pile-up is defined as the total charge collected in a detector which is recorded as a single event but is actually the summed charge deposited by two events. For ^{10}B profiles in $Hg_{1-x}Cd_xTe$, pulse pile-up

is the sum of the energy deposited from the occasional α-particle that originates from the $^{10}B(n, \alpha)\ ^{7}Li$ reaction and a partial energy deposition from the numerous electrons emitted from the cadmium constituents. Consequently, the measured charged-particle spectra from the $Hg_{1-x}Cd_xTe$ samples are broadened beyond the normal total system resolution for an ideal material. Despite the large cross section for neutron absorption in these samples, the volume analyzed remains uniformly illuminated with neutrons. Thus, the profiles are not distorted due to neutron self-shielding over the depth of the profile. To provide an independent quality control check, a constant precision pulser signal is also fed to the input of the detector preamplifier to monitor any shifts in the overall system electronics. The pulser signal indicated that shifts in the spectral energy scale were input equivalent to less than 1 nm of depth. In addition, this procedure provides a monitor for the severity of pulse pile-up effects to the NDP analyses.

Several representative ^{10}B distributions that were obtained by NDP are shown in Figs. 3-6. These plots have not been corrected for either the pulse pile-up effect or system resolution. Consequently, the ^{10}B distributions have been broadened toward the shallower depths and even extend somewhat above the sample surfaces as can be seen in Figs. 3-6. Nevertheless, several interesting observations and conclusions can be made from these plots in their present form since pulse pile-up does not affect the reproducibility of the spectra or the quantitative determination of the total boron concentration. This latter point is amply demonstrated by the excellent agreement between the NDP measured boron contents in Table 2 and the quantities actually implanted (i.e., 2.0×10^{15} B ions/cm^2). Procedures to accurately correct these NDP profiles for the pulse pile-up contributions are currently being developed.

The boron profiles for low-energy (i.e., 40 and 100 keV) implants are illustrated in Figs. 3 and 4. Although the ^{10}B maximum occurs more than 100 nm below the bare $Hg_{0.7}Cd_{0.3}Te$ surface in sample NDP-3, the ^{10}B peaks in NDP-1 (not shown) and NDP-2 lie just below the interfaces with the SiO_2 films. These profile differences produce two significant features: (1) as summarized in Table 2, approximately 30% of the implanted ^{10}B actually remains in the SiO_2 layers and cannot affect the electrical properties of the $Hg_{1-x}Cd_xTe$

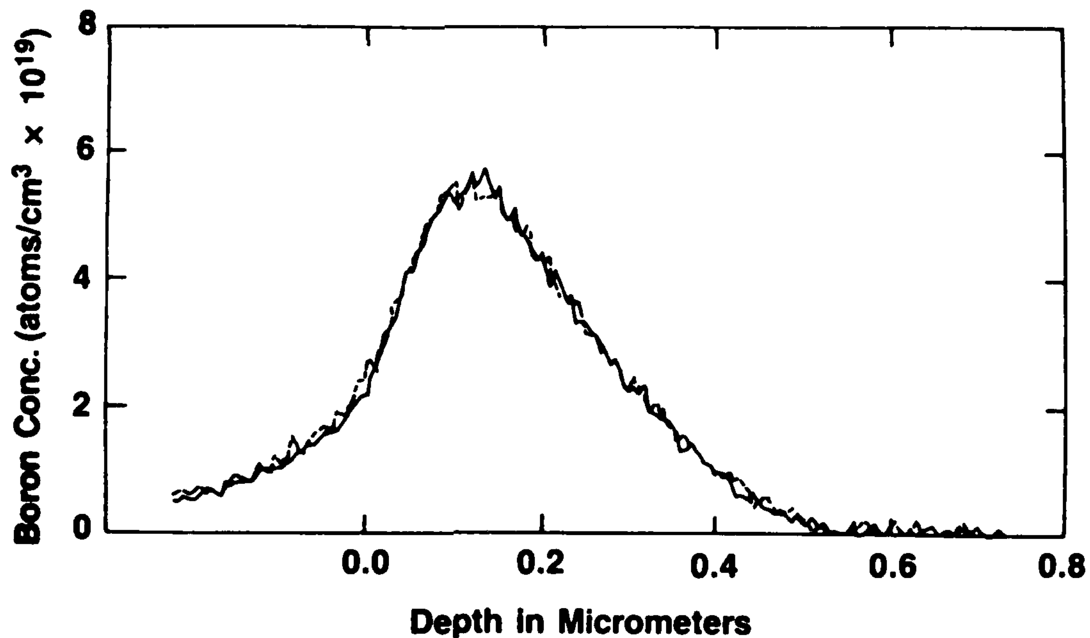

Fig. 3. ^{10}B profiles for $Hg_{0.68}Cd_{0.32}Te$ sample NDP-3 as implanted (solid curve) and after 1 hr 200°C anneal (dashed line).

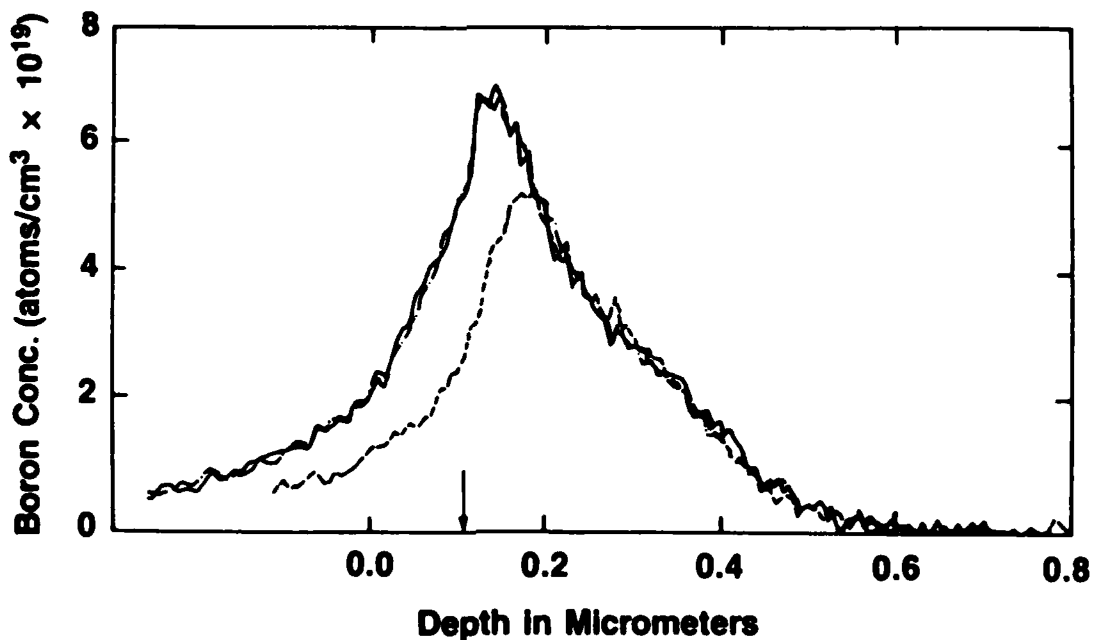

Fig. 4. ^{10}B profiles for PC-SiO_2 coated $Hg_{0.68}Cd_{0.32}Te$ sample NDP-2 as implanted (——), after 1 hr 200°C anneal (.-.-.), and after buffered HF etch (---) to remove SiO_2 film. This last curve was shifted by 1.05 μm to align deeper profiles and permit estimate of SiO_2 film thickness, which is marked by the arrow.

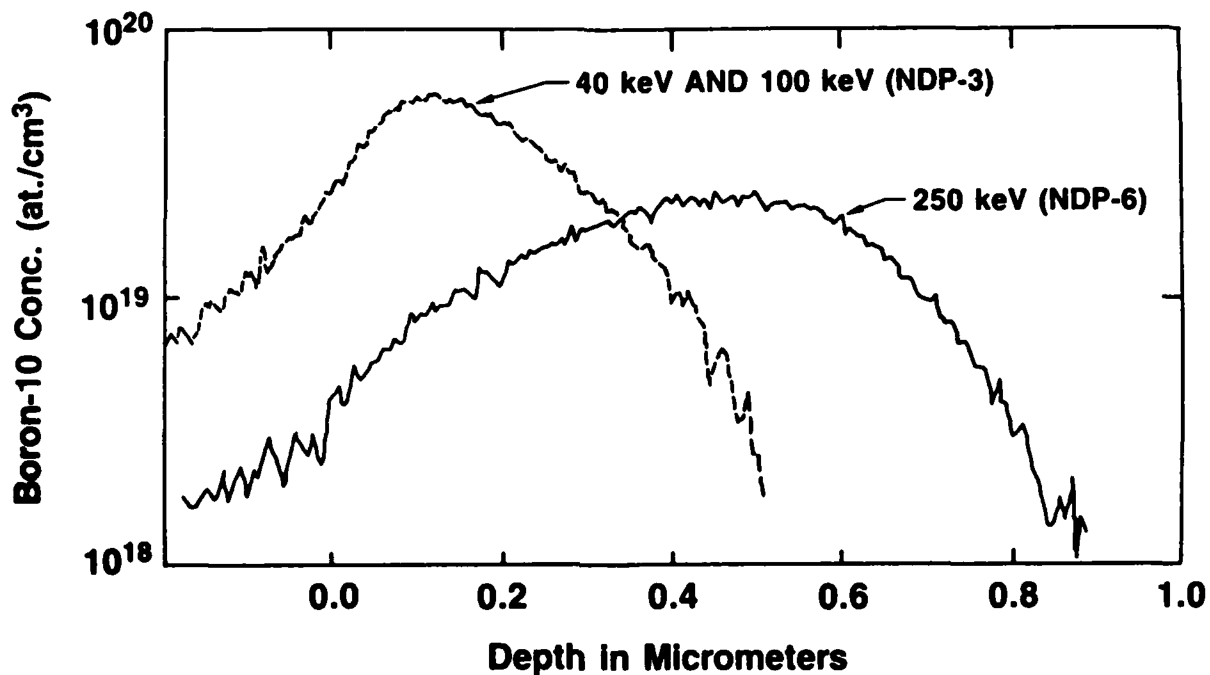

Fig. 5. Comparison of ^{10}B profiles for different implant energies.

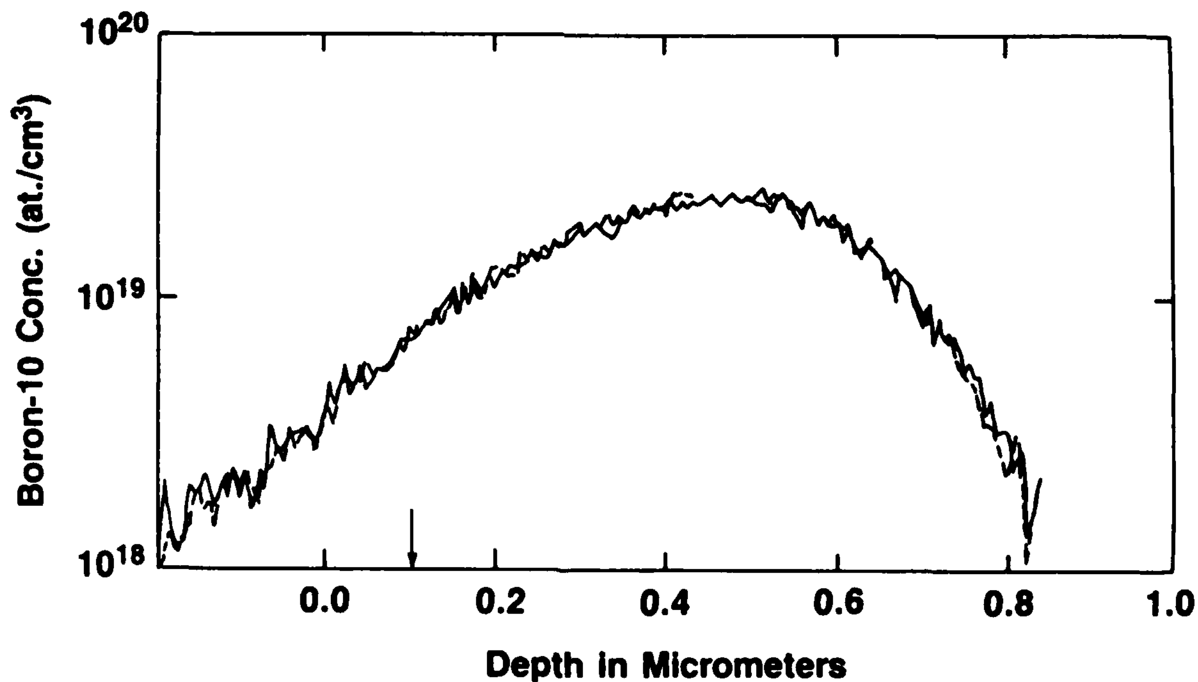

Fig. 6. Measured ^{10}B profiles for as-implanted 250 keV $^{10}B^{+}$ ions in bulk sample NDP-5 (solid curve) and epitaxial sample NDP-7 (dashed curve). The arrow denotes the SiO_2-$Hg_{0.7}Cd_{0.3}Te$ interface determined by ellipsometry.

substrate and (2) a boron concentration peak occurs at the $Hg_{0.7}Cd_{0.3}Te$ surface in samples covered by the SiO_2 film. This enhanced boron content correlates very well with the larger N_e carrier ratio previously shown in Fig. 2. While specific contributions of the implanted boron ions to n-p junction formation in $Hg_{1-x}Cd_xTe$ have not been established, it is widely held[1-3] that various defects created by the implantation process are mainly responsible for generating the donor states. However, comparison of the present NDP and Hall data implies that at least partial electrical activation of the implanted boron may occur since the larger surface boron contents directly correspond to increased N_e densities. An alternative explanation would involve more defects being produced by the greater number of stopped boron atoms. Additional correlation studies are needed to settle this issue. However, Figs. 3 and 4 also clearly show that the often used 200°C anneals have no detectable influence on the implanted boron distribution in either the SiO_2 or $Hg_{0.7}Cd_{0.3}Te$ regions.

Figure 5 shows the effects of implant energy on the ^{10}B profiles in epitaxial $Hg_{0.7}Cd_{0.3}Te$ samples. In agreement with previous results,[7] the 250 keV implants produce a broader and lower amplitude ^{10}B peak that is much deeper into the material than is found for the combined 40 keV and 100 keV implants. Figure 6 compares the ^{10}B distribution for 250 keV implants through nominal 100 nm SiO_2 films on epitaxial (NDP-6) and bulk (NDP-5) $Hg_{0.7}Cd_{0.3}Te$ samples. No significant differences are seen where both ^{10}B profiles are asymmetric with larger boron levels toward the surface. However, these higher energy implants leave only small quantities of boron in the SiO_2 films and no discontinuities can be discerned at the interface with the $Hg_{0.7}Cd_{0.3}Te$ substrate. Nevertheless, the ^{10}B peak occurs almost 100 nm deeper in the bare surface sample NDP-6, which is almost identical to the SiO_2 film thickness. Hence, the as-implanted boron distribution is essentially identical (within the present resolution limits) in SiO_2 and in $Hg_{0.7}Cd_{0.3}Te$.

IV. CONCLUSIONS

In summary, the present NDP and Hall measurements indicate some substantial differences can occur when boron ions are implanted through nominal 100 nm PC-SiO_2 films rather than directly into the freshly etched HgCdTe surfaces. For example, only portions of low-energy (i.e., 40 keV and 100 keV) implants actually penetrate the SiO_2 films to form rather shallow n-p junctions which may cause variations in photodiode performance. Deeper junctions require higher implant energies to compensate for the presence of the SiO_2 films. Although 200°C anneals do not alter the ^{10}B profiles, they may change device properties by modifications of other defects in either the $Hg_{1-x}Cd_xTe$ or SiO_2 layers. Additional studies are currently in progress to assess possible changes and will be reported elsewhere.

REFERENCES

1. M. B. Reine, A. K. Good, and T. J. Tredwell, "Photovoltaic Infrared Detectors," in Semiconductors and Semimetals, Vol. 18, edited by R. K. Willardson and A. C. Beer, Academic Press, New York, 1981, pp. 201-311.

2. G. L. Destefanis, Nucl. Instrum. Methods 209/210, 567-80 (1983).

3. T. W. Sigmon, Nucl. Instrum. Methods B7/8, 402-8 (1985).

4. B. K. Janousek, R. C. Carscallen, and P. A. Bertrand, J. Vac. Sci. Technol. A1, 1723-25 (1983).

5. B. K. Janousek and R. C. Carscallen, J. Vac. Sci. Technol. A3, 195-98 (1985).

6. J. F. Wager and D. R. Rhiger, J. Vac. Sci. Technol. A3, 212-17 (1985).

7. H. Ryssel, K. Mueller, J. Biersack, W. Kruger, G. Lang, and F. Jahnel, Phys. Status Solidi A 57, 619-24 (1980).

8. R. G. Downing, R. F. Fleming, J. K. Lang, and D. H. Vincent, Nucl. Instrum. Methods 218, 47-51 (1983).

9. R. G. Downing, J. T. Maki, and R. F. Fleming, Microelectronic Processing: Inorganic Materials Characterization-A.C.S. Symp. Ser. 295, edited by L. A. Casper, Am. Chem. Soc., Washington, D. C., 1986, pp. 163-80.

10. L. F. Lou and W. H. Frye, J. Appl. Phys. 56, 2253-67 (1984).

11. D. D. Edwall, E. R. Gertner, and W. E. Tennant, J. Appl. Phys. 55, 1453-60 (1984).

12. S. H. Shin, E. R. Gertner, J. G. Pasko, and W. E. Tennant, J. Appl. Phys. 57, 4721-26 (1985).

13. J. F. Ziegler, G. W. Cole and J. E. Baglin, J. Appl. Phys. 43, 3809-15 (1972).

14. J. P. Biersack, D. Fink, R. Henkelmann, and K. Muller, Nucl. Instrum. Methods 149, 93-97 (1978).

LABORATORY OPERATIONS

The Aerospace Corporation functions as an "architect-engineer" for national security projects, specializing in advanced military space systems. Providing research support, the corporation's Laboratory Operations conducts experimental and theoretical investigations that focus on the application of scientific and technical advances to such systems. Vital to the success of these investigations is the technical staff's wide-ranging expertise and its ability to stay current with new developments. This expertise is enhanced by a research program aimed at dealing with the many problems associated with rapidly evolving space systems. Contributing their capabilities to the research effort are these individual laboratories:

Aerophysics Laboratory: Launch vehicle and reentry fluid mechanics, heat transfer and flight dynamics; chemical and electric propulsion, propellant chemistry, chemical dynamics, environmental chemistry, trace detection; spacecraft structural mechanics, contamination, thermal and structural control; high temperature thermomechanics, gas kinetics and radiation; cw and pulsed chemical and excimer laser development including chemical kinetics, spectroscopy, optical resonators, beam control, atmospheric propagation, laser effects and countermeasures.

Chemistry and Physics Laboratory: Atmospheric chemical reactions, atmospheric optics, light scattering, state-specific chemical reactions and radiative signatures of missile plumes, sensor out-of-field-of-view rejection, applied laser spectroscopy, laser chemistry, laser optoelectronics, solar cell physics, battery electrochemistry, space vacuum and radiation effects on materials, lubrication and surface phenomena, thermionic emission, photo-sensitive materials and detectors, atomic frequency standards, and environmental chemistry.

Computer Science Laboratory: Program verification, program translation, performance-sensitive system design, distributed architectures for spaceborne computers, fault-tolerant computer systems, artificial intelligence, micro-electronics applications, communication protocols, and computer security.

Electronics Research Laboratory: Microelectronics, solid-state device physics, compound semiconductors, radiation hardening; electro-optics, quantum electronics, solid-state lasers, optical propagation and communications; microwave semiconductor devices, microwave/millimeter wave measurements, diagnostics and radiometry, microwave/millimeter wave thermionic devices; atomic time and frequency standards; antennas, rf systems, electromagnetic propagation phenomena, space communication systems.

Materials Sciences Laboratory: Development of new materials: metals, alloys, ceramics, polymers and their composites, and new forms of carbon; non-destructive evaluation, component failure analysis and reliability; fracture mechanics and stress corrosion; analysis and evaluation of materials at cryogenic and elevated temperatures as well as in space and enemy-induced environments.

Space Sciences Laboratory: Magnetospheric, auroral and cosmic ray physics, wave-particle interactions, magnetospheric plasma waves; atmospheric and ionospheric physics, density and composition of the upper atmosphere, remote sensing using atmospheric radiation; solar physics, infrared astronomy, infrared signature analysis; effects of solar activity, magnetic storms and nuclear explosions on the earth's atmosphere, ionosphere and magnetosphere; effects of electromagnetic and particulate radiations on space systems; space instrumentation.

...

END
8-87
DTIC